Supporting Information for

Heterogeneous Three-dimensional FeSiAl@SiO_2@MoS_2 Composite with a SiO_2 Wave-transmitting Layer for Enhanced Electromagnetic Wave Absorption Performance

Yige Han [a], Feng Chen [a]*, Qiang Fu [a]*

[a] College of Polymer Science and Engineering, Sichuan University, Chengdu 610065, China

* Corresponding author: Feng Chen (fengchen@scu.edu.cn); Qiang Fu (qiangfu@scu.edu.cn).

1. Computer Simulation Technology (CST)

CST software was employed for simulating radar cross section (RCS) at 14.24 GHz. RCS serves as a metric for assessing the detectability of radar targets. Lower RCS values correspond to enhanced EMWA capabilities of the absorber. The RCS values (σ) can be quantified using the following formula:

$$\sigma(dB\ m^2) = 10\log\left(\frac{4\pi S}{\lambda^2}\left|\frac{E_s}{E_i}\right|\right)^2$$

Where S is the area of the model, and E_s and E_i represent the electric field intensities of scattered and incident waves, respectively.

1.1 RCS of the vertical plate model

The width of the model was 100 mm×100 mm and the thicknesses of the materials corresponded thicknesses of best EMWA performance, while the thickness of the PEC plate was 0.1 mm. With the change in the angle of incidence, it leads to significant fluctuations in the RCS of the samples[1].

1.2 Electromagnetic field intensity distribution (V/m) and Power loss density (W m^{-3})

The electromagnetic wave propagates from left to right. On the left side of the absorbing film, the initial electromagnetic signal intensity remains unabsorbed. However, on the right side, there is a noticeable attenuation of the electromagnetic signal compared to the left side. This observation indicates a substantial absorption of electromagnetic waves, showcasing the material's robust EMWA capability.

The variation in power loss density is closely linked to the attenuation of electromagnetic waves within the absorber. A higher simulation result of power loss

density signifies superior attenuation capabilities[2].

1.3 RCS of the drone model

To demonstrate the potential of the absorber for military applications, the drone model was constructed using CST software, and its RCS values were computed at 10 GHz. The absorption properties of the coating were simulated in military radar stealth scenarios, yielding the RCS characteristics under both TE and TM polarizations.

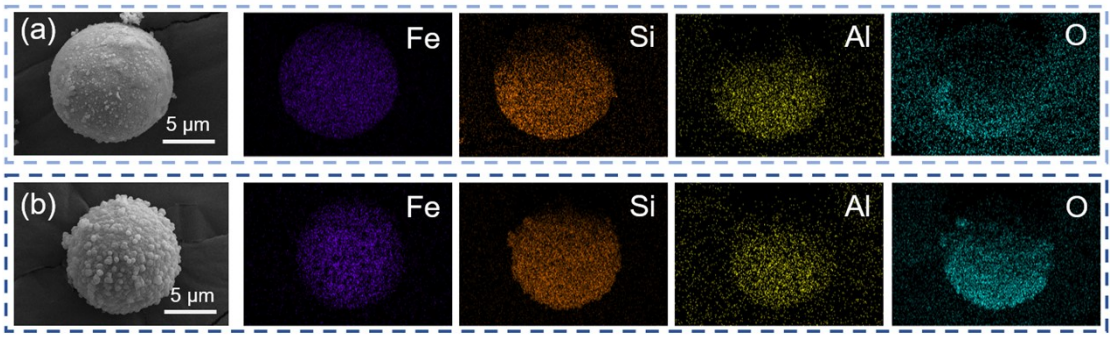

Fig. S1. SEM images and element mapping of the FSO-1 (a), FSO-2 (b).

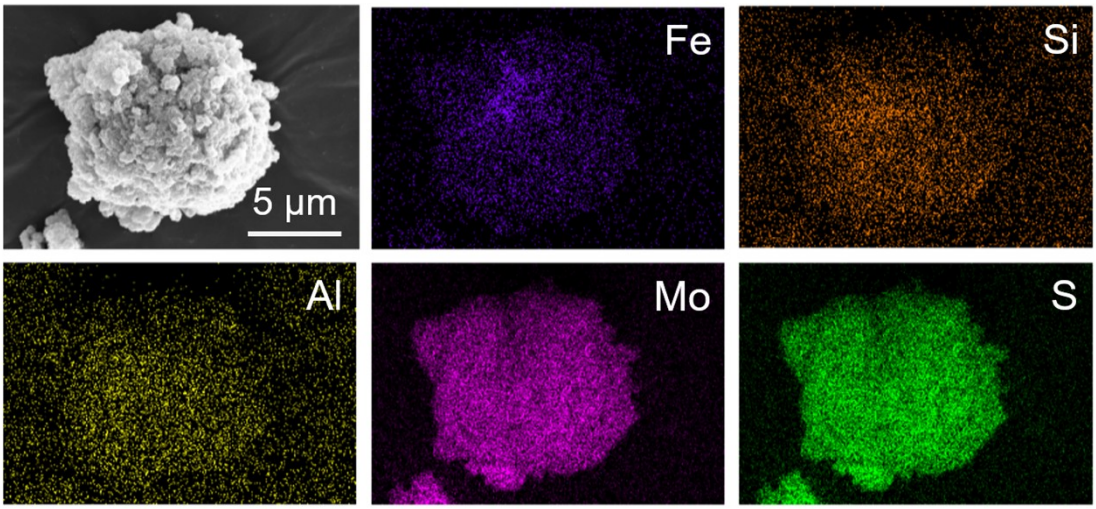

Fig. S2. SEM image and element mapping of the FeSiAl@MoS_2 (FSAM).

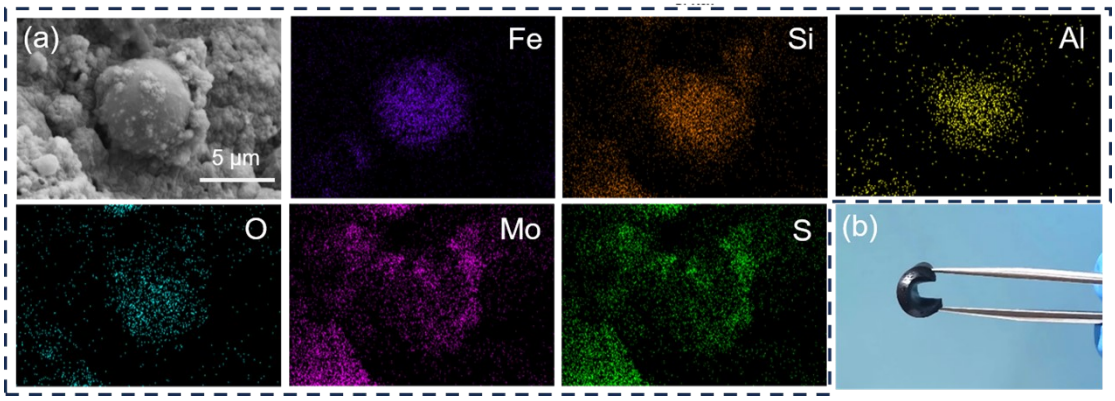

Fig. S3. SEM image and element mapping (a) and Digital photograph (b) of the FeSiAl@SiO_2@MoS_2/SR.

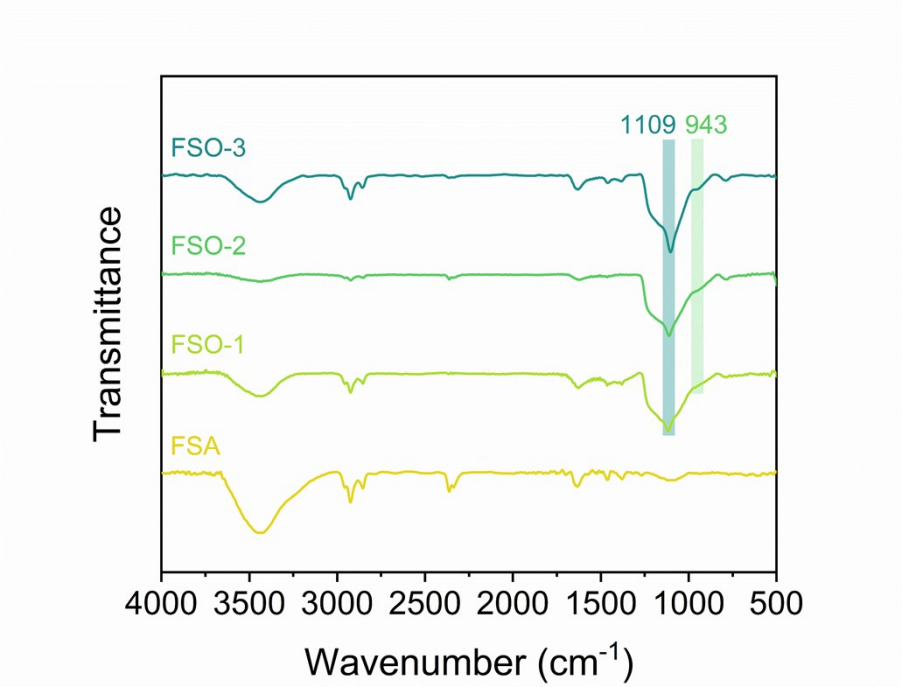

Fig. S4. FTIR spectra of FSA, FSO-1, FSO-2 and FSO-3.

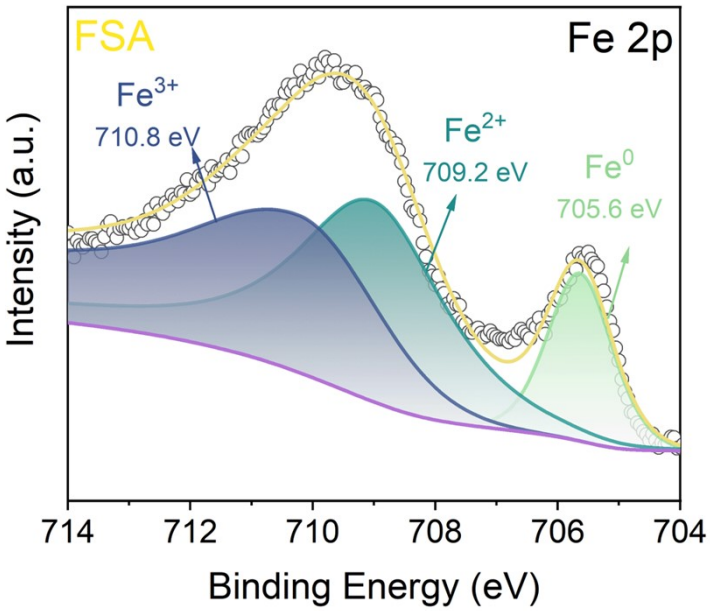

Fig. S5. XPS spectra of Fe 2p of FSA.

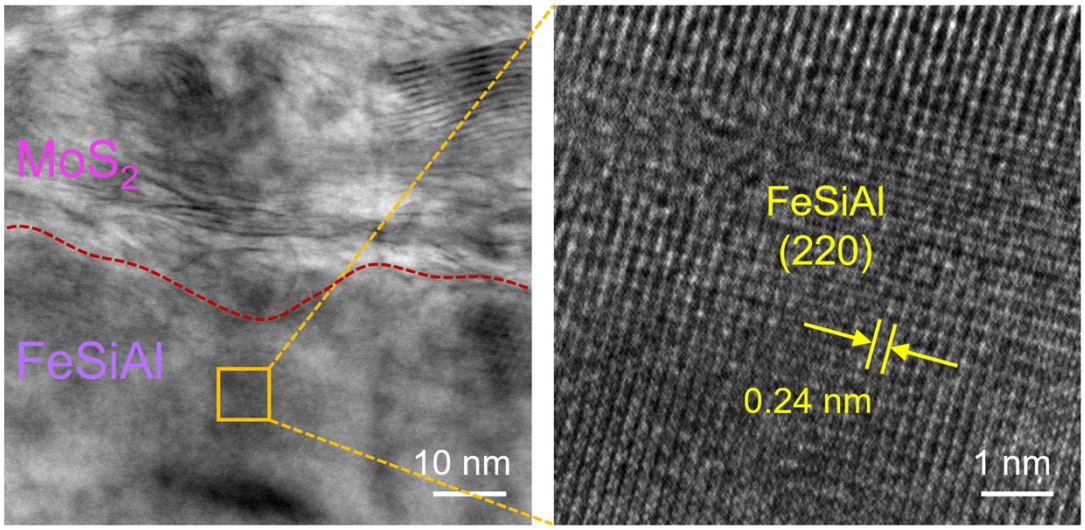

Fig. S6. HRTEM images of FSOM-2 (including MoS_2 and FeSiAl interface).

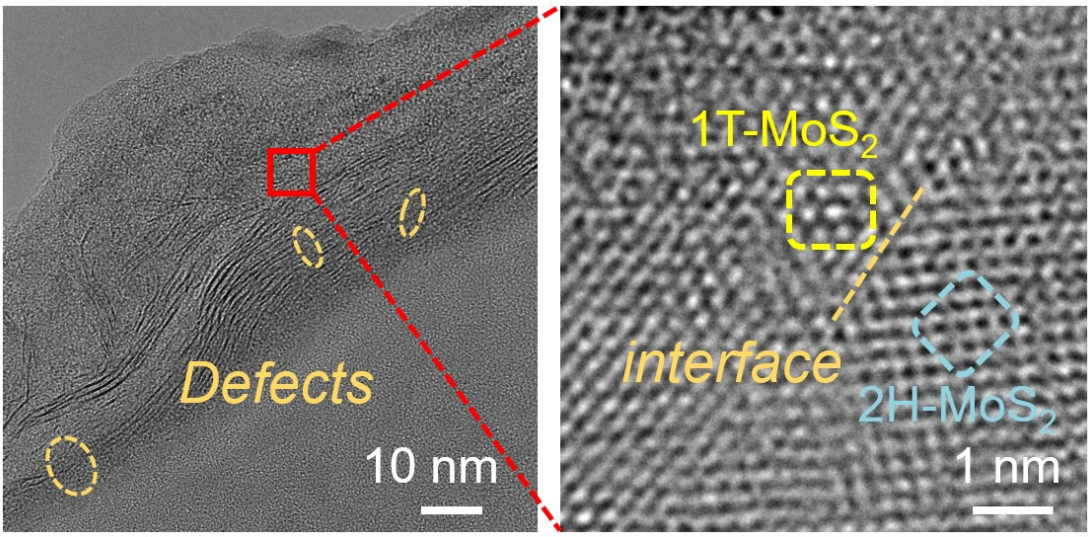

Fig. S7. HRTEM images of FSOM-2 (including two phases of MoS_2).

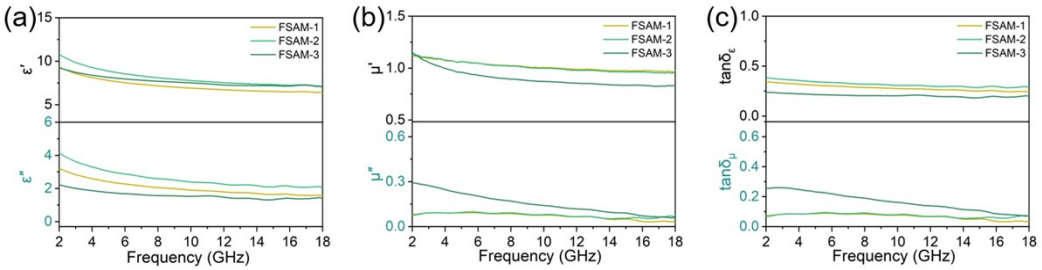

Fig. S8. Real and imaginary parts of complex permittivity (a) and complex permeability (b), Dielectric loss tangent, and magnetic loss tangent (c) of FSAM-1, FSAM-2, and FSAM-3.

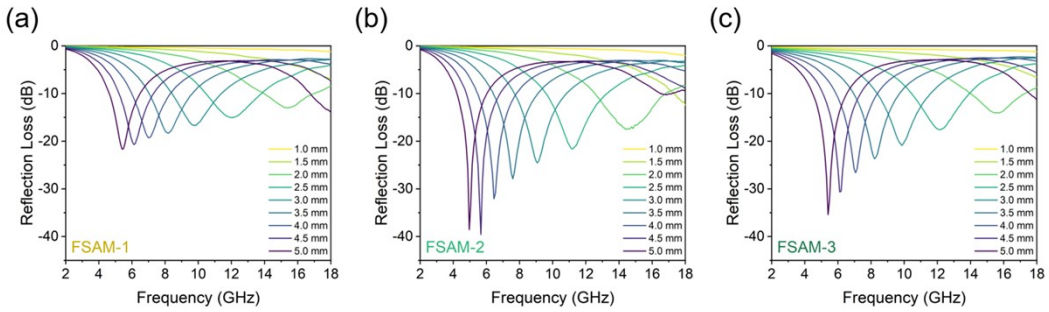

Fig. S9. RL curves (a-c) of FSAM-1, FSAM-2 and FSAM-3.

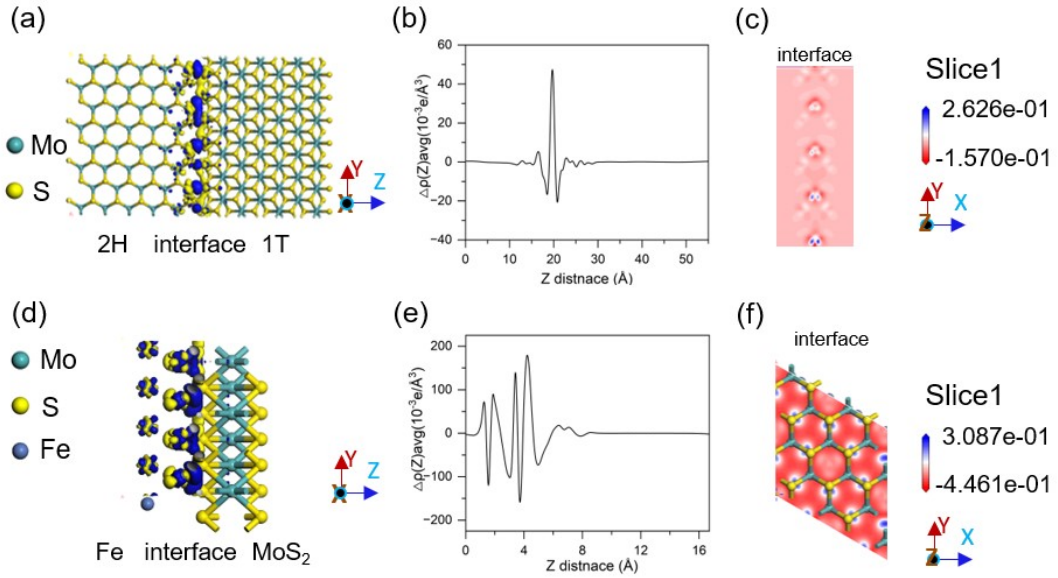

Fig. S10. Charge density difference plot of 1T MoS_2-2H MoS_2 (a-c), and Fe-MoS_2 (d-f). The blue and yellow regions represent electron depletion and electron accumulation, respectively.

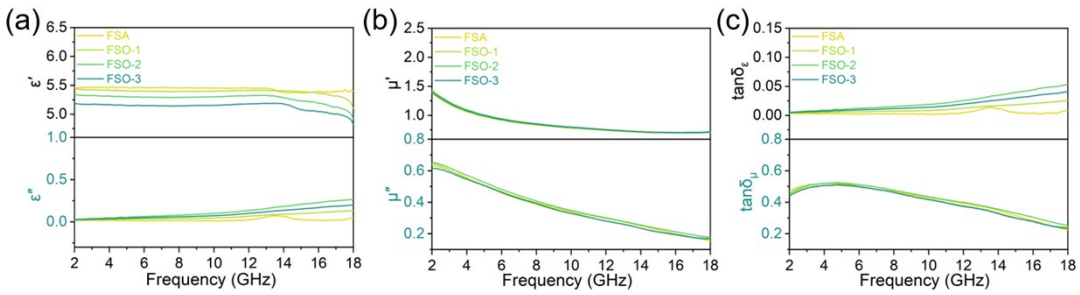

Fig. S11. Real and imaginary parts of complex permittivity (a) and complex permeability (b), Dielectric loss tangent, and magnetic loss tangent (c) of FSA, FSO-1, FSO-2, and FSO-3.

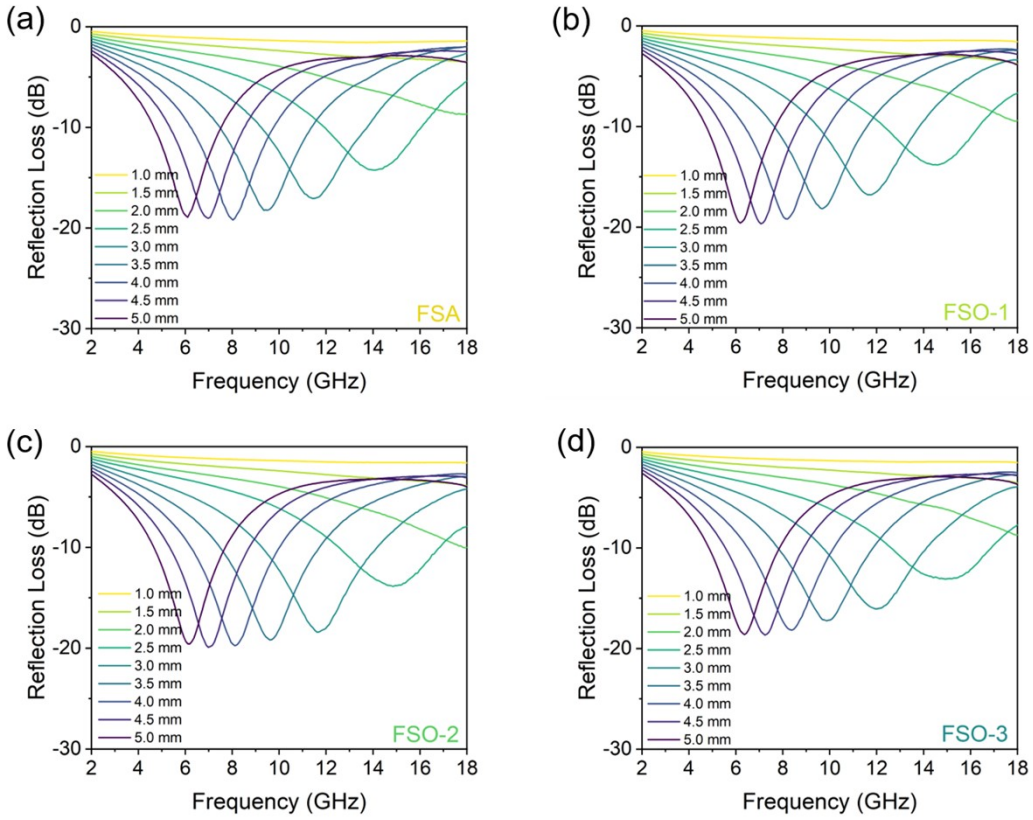

Fig. S12. RL curves (a-d) of FSA, FSO-1, FSO-2 and FSO-3.

Table S1. The contrast of microwave absorption properties with other reported absorbers

Absorbers	RL_{min} (dB)	Matching thickness (mm)	EAB_{max} (GHz)	Matching thickness (mm)	Reference
Co_xS_y/C@MoS_2	−41.32	3.3	3.67	3.7	3
Fe_3O_4/Fe@C@MoS_2	−53.79	2.24	4.4	2.24	4
MoS_2/Fe_3O_4/PANI	−50.3	2.6	5.1	1.8	5
FeSiAl/NiZn ferrite	−29.2	2.5	3.75	2.5	6
FeSiAl/graphite	−21.0	3.0	2.4	1.5	7
FeSiAl/Al_2O_3	−34.2	1.9	1.9	1.9	8
FeSiAl/ZnO	−50	2.4	3.5	2.2	9
Fe@MoS_2	−37.02	2.0	4.73	2.0	10
MoS_2/Mxene/NC	−52.9	3.4	5.2	1.6	11
MoS_2/TiO_2/Ti_2CT_x	−54.70	3.39	4	2.0	12
FSOM-2	−66.8	1.96	5.22	1.86	This work

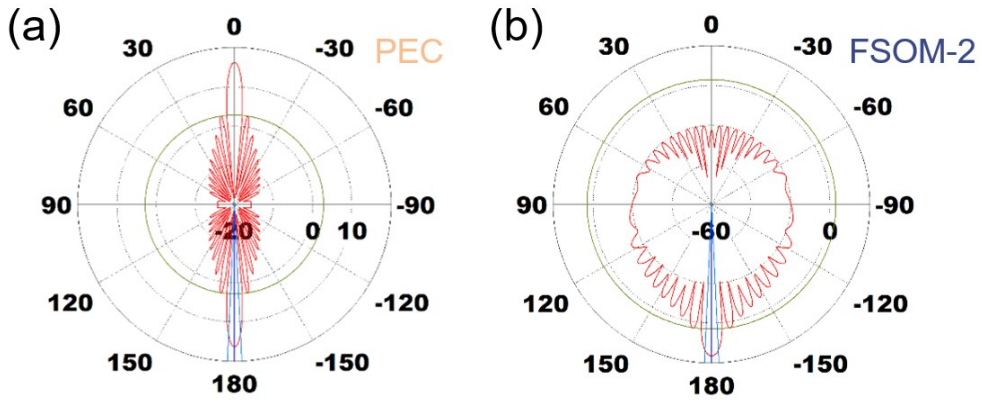

Fig. S13. 2D radar wave scattering signals of PEC and FSOM-2.

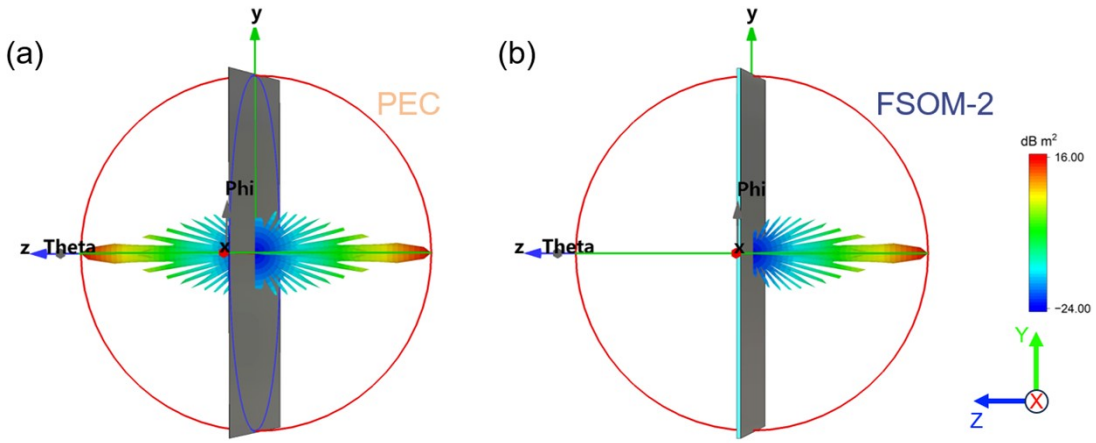

Fig. S14. 3D radar wave scattering signals of PEC and FSOM-2.

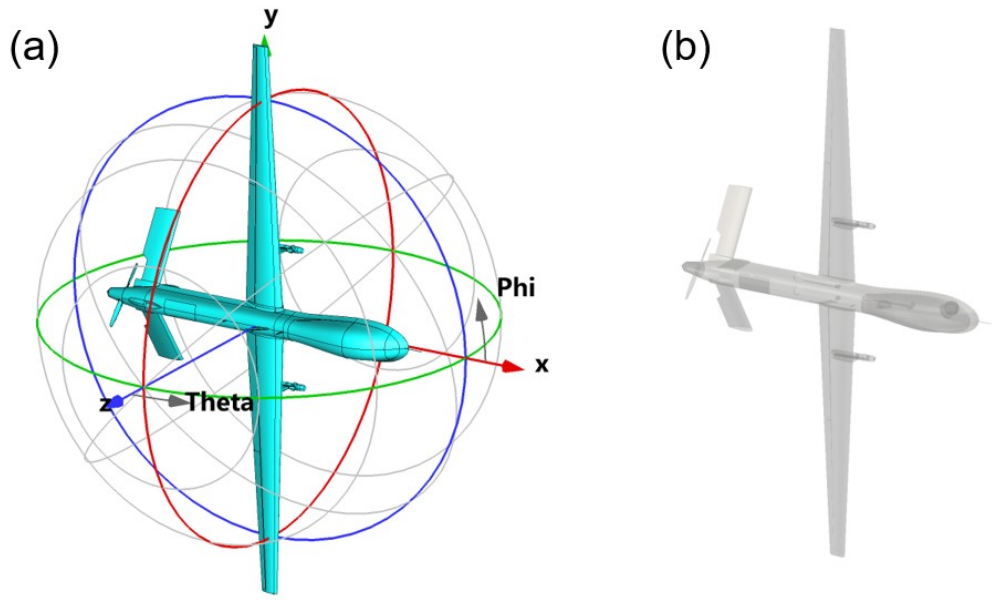

Fig. S15. The Drone simulates the RCS process in the CST Studio Suite 2023 software (a); Location of stealth coating on the drone (b).

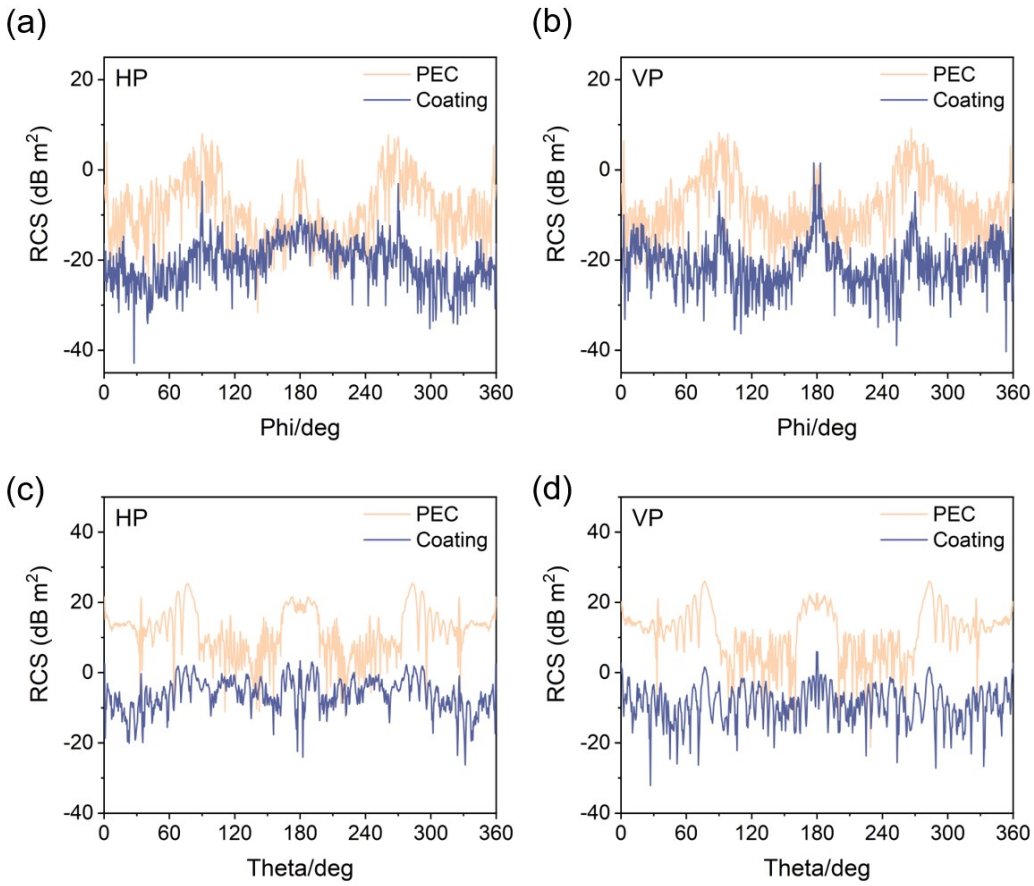

Fig. S16. Forward and Top views RCS curves of the drone at 10 GHz under horizontal polarization (a, c) and vertical polarization (b, d) of PEC and FSOM-2 coating.

References

1 W. Gu, S. J. H. Ong, Y. Shen, W. Guo, Y. Fang, G. Ji and Z. J. Xu, Adv. Sci., 2022, **9**, 2204165.

2 J. Xu, M. Liu, B. Li, X. Zhang, X. Zhang, C. Zhu and Y. Chen, Appl. Phys. Rev., 2022, **9**, 011402.

3 Q. Zhu, X. Zhang, Y. Zheng, Y. Xia, Z. Nie, W. Zhang, H. Yan and S. Qi, J. Mater. Sci.: Mater. Electron., 2020, **32**, 25782–25794.

4 Z. Tong, Z. Liao, Y. Liu, M. Ma, Y. Bi, W. Huang, Y. Ma, M. Qiao and G. Wu, Carbon, 2021, **179**, 646–654.

5 X. Wang, C. Li, H. Geng, J. Xie, Z. Chen, X. Zhang, C. Xiong and S. Wang, Colloids Surf. A, 2022, **637**, 128285.

6 C. Lei and Y. Du, J. Alloys Compd., 2020, **822**, 153674.

7 J. Sun, H. Xu, Y. Shen, H. Bi, W. Liang and R. Yang, J. Alloys Compd., 2013, **548**, 18–22.

8 L. Zhou, J. Huang, X. Wang, G. Su, J. Qiu and Y. Dong, J. Alloys Compd., 2019, **774**, 813–819.

9 L. Zhou, J. Huang, H. Wang, M. Chen, Y. Dong and F. Zheng, J. Mater. Sci.: Mater. Electron., 2018, **30**, 1896–1906.

10 J. Pan, X. Sun, T. Wang, Z. Zhu, Y. He, W. Xia and J. He, Appl. Surf. Sci., 2018, **457**, 271–279.

11 Y. Fan, Z. Liu, Q. Li, K. Zhao, M. Ahmad, P. Liu, Q. Zhang and B. Zhang, ACS Appl. Mater. Interfaces, 2023, **15**, 41720–41731.

12 B. Miao, Y. Cao, Q. Zhu, M. A. Nawaz, J. A. Ordiozola, T. R. Reina, Z. Bai, J. Ren and F. Wei, Adv. Compos. Hybrid Mater., 2023, **6**, 61.